Jurnal Fizik Malaysia Volume 43 Issue 1 (2022) pgs 10131-10138 T. E. Lim

Initial Stages of Yttria Stabilized Zirconia Nucleation: A Combined Experimental-Simulation Approach

Lim Tian Earng, R. Muhammad and Wong Siew Ying

Department of Physics, Faculty of Science, University of Teknologi, 81310 UTM, Skudai, Johor, Malaysia.

(Received: 18.12.21 ; Published: 16.6.22)

Abstract. In this work, the initial stage of nucleation of yttria stabilized zirconia (YSZ) was investigated by using a computer program and parameters such as critical radius, (r^*) critical free energy, (ΔG^*) and so on were studied. As a first step toward to this work, the YSZ thin film sintered at 1100°C−1500°C were investigated using Atomic Force Microscopy (AFM) and X-Ray Diffraction (XRD). The grain size and microscopic asperity of the surface texture and several parameters such as crystallite size, lattice parameter and microstrain of YSZ thin film have been studied. It was found that the YSZ thin film follow the Volmer-Weber growth mode and the temperature and contact angle can influence the surface energy of the solid nucleus which eventually change the ΔG^* and r^*.

Keywords: YSZ, morphology, microstrain, surface roughness

I. INTRODUCTION

Nanotechnology is concerned with development and utilization of structures and devices with organizational features at the nanoparticle scale and it remains the most significant part in the creation of any nanostructure [1-2]. Zirconia (ZrO_2) nanoparticles is applicable for a wide-ranging of industrial purpose such as solid electrolytes for fuel cells due to its remarkable properties such as excellent refractoriness, high ionic conductivity, high thermal expansion coefficient and good thermal stability [3]. The atomic structure, composition and characteristic defects of YSZ surfaces are key to a basic understanding of this application relevant material [4]. ZrO_2 own three different crystalline structures which are cubic, tetragonal and monoclinic polymorphs. The monoclinic phase stable at room temperature, it then transformed to tetragonal at 1170 °C, and then to cubic at 2370 °C. However, to make it applicable in fields that does not have such high temperature, many divalent and trivalent cationic species such as Mg^{2+}, Ca^{2+}, and Y^{3+} have been incorporated into ZrO_2 to prepare cubic and tetragonal zirconia that is stable at room temperature [5]. As such that the study on the YSZ nanoparticles in term of preparation method and structural properties are important to the deposition of YSZ thin film.

The initial stage of the nucleation process is especially important in the deposition of thin film. The nucleation process plays important role to material science especially on describing the change of phase of a material in nanoscale. In this work, in contemplation of enhancing the understanding on the theory of nucleation and growth mechanism of the YSZ nanoparticles, the Atomic Force Microscopy (AFM) and X-Ray Diffraction (XRD) were used in the experiment to get further understanding on the morphology and microstructure characteristics of YSZ film synthesized using sol-gel method.

Paper contributed to the National Physics Conference 2021 (PERFIK2021), 29 – 30 June 2021

II. METHODOLOGY

The thin film YSZ samples were prepared using sol-gel method. At first, the zirconium (IV) oxynitrate hydrate ($ZrO(NO_3)_2 \cdot 2H_2O$) and yttrium nitrate ($Y(NO_3)_3 \cdot 6H_2O$) with appropriate amount will need to be dissolved in 80 ml of citric acid at 80 °C. The solvent then undergoes slow evaporation and transparent gels will be obtained. These concentrated Y–Zr–O nitrate–citrate gels then diluted with ethanol with ratio of (1:4). The obtained Y–Zr–O gels will then be used for the preparation of the YSZ coatings by spin-coating technique. The 0.1 ml of gel solution was dripped on the glass substrate (SiO_2) and spun for 40 s using a spinning rate of 2000 rpm. The obtained thin films of YSZ were heated at 400 °C for 10 min after each coating. Finally, after the third coating procedure the obtained materials were sintered for 5 h at 1100 °C. 5 set of samples were prepared by increasing the sintering temperature which are 1100 °C, 1200 °C, 1300 °C, 1400 °C, 1500 °C and labelled as sample code S1, S2, S3, S4, S5.

The microstructure of the YSZ thin film were determined by using XRD. The XRD pattern of the sample code S1, S2, S3, S4 and S5 will be obtained using XRD and several parameters such as crystallite size, lattice parameter and microstrain of YSZ thin film will be calculated. For the surface morphology of the YSZ thin film, AFM will be used to analyse and obtain the 3-dimensional AFM images and from the AFM images the average surface roughness, root mean square roughness and grain size were obtained.

Apart from that, a simulation by using a computer program call Microsoft Visual Basic is done to investigate the initial stage of nucleation of YSZ and parameters such as critical radius, (r^*) critical free energy, (ΔG^*) and so on were studied. The simulation data will then be plot by using a plotting computer program, Gnuplot.

III. RESULTS AND DISCUSSION

XRD

The figure 1 shows the results of XRD patterns for all the YSZ thin films sample code S1, S2, S3, S4 and S5. The XRD patterns were conducted under the room temperature in purpose to confirm the phase of the sample. The XRD patterns demonstrate the crystallinity and major orientation of YSZ films synthesized onto the glass substrate. By analysing the XRD patterns of S1, S2 and S3 from the Figure 1 (a), it can be seen that the XRD patterns of the prepared samples were in single phase and exhibit the cubic structure with Fm-3m space group. Furthermore, when the sample has been sintered up until 1300 °C, the highest intensity peak appears with the hkl parameters of the different peak for all the samples were indexed to (111), (200), (220) and (311). From the magnification picture, Figure 1 (a) at the plane (100) and (200), it is apparent that the reflection peaks intensity and peak broadening will increase as the sintering temperature rise to 1300 °C and this situation implying the reduction of crystallinity. Based on the Figure 1 (b), the sintering temperature increase up to 1500 °C, the intensity peak for (111) in S4 and S5 continue increasing compared to S1 to S3 but there is another peak appeared near this main peak side by side and this peak is identified as baddeleyite. The show up of the Baddeleyite peak at 1400 °C and 1500 °C may be because of excessive heating while preparing the suspension. The existence of Baddeleyite eventually give an effect and show uneven fluctuation result in strain, lattice parameter and crystallite size.

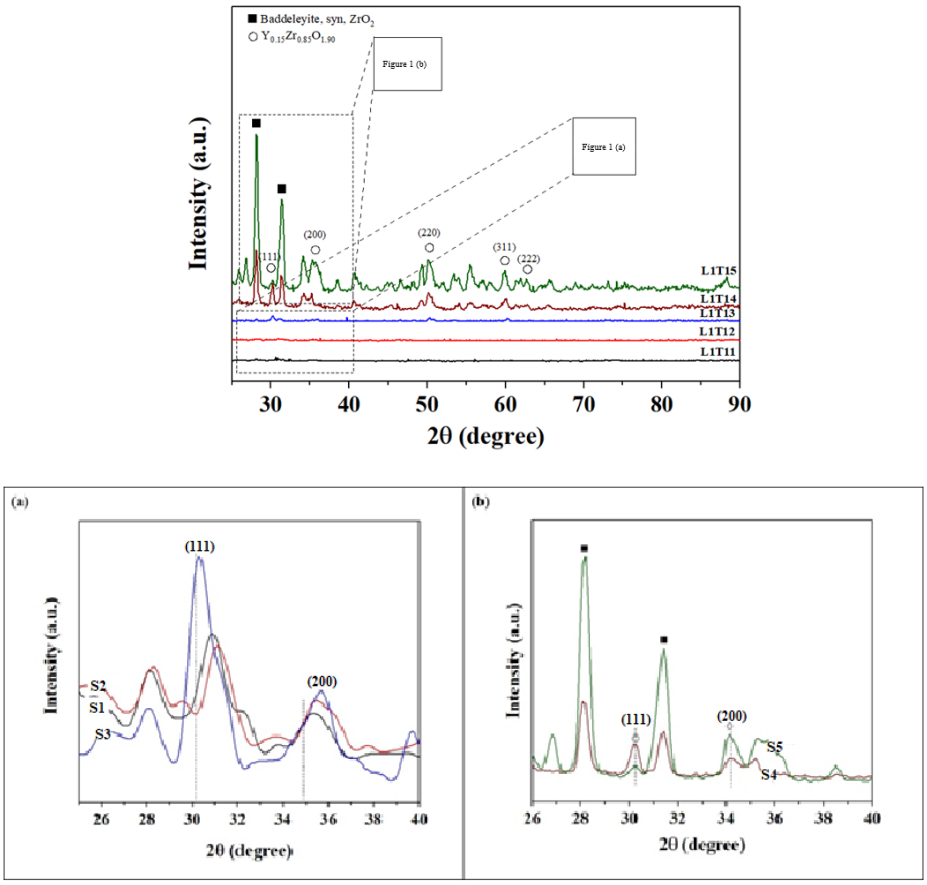

FIGURE 1. The XRD pattern of YSZ thin film with variable sintered temperature S1, S2, S3, S4 and S5. (a) Peak shift of S1, S2 and S3 at (111) and (200). (b) Peak shift of S4 and S5 at (111) and (200).

The uneven fluctuations of crystallite size, τ, lattice parameter, a and microstrain, σ as the sintering temperature increase were tabulated into Table 1. The mean crystallite size was calculated followed the Scherrer equation in equation (3) using the full width at half maximum (FWHM) obtained from diffraction pattern [6]. The alter of microstrain and defect in phase structure contribute to the effect of lattice parameter expands and shrank during rising sintering temperature. The alter of microstrain clarified the root means square of the variations in the lattice parameters across the sample. There is also deformation contribute to the local distortion of lattice planes which then give rise to nonuniform variation in the interplanar spacings. The positive value of microstrain explained the distance of the relevant crystal planes is not identical. Moreover, the alter in microstrain and the lattice parameter generally follow a similar dependence on the grain size. Change in sintering temperature leads to the difference in thermal and mechanical properties of the film. The defects in crystallography of film leading to the higher resistance especially for ion transportation for ionic conductivity performance. The value of microstrain was calculated from the equation of Williamson-hall given by equation (4) [7]. The equation to calculate the lattice parameter of the cubic YSZ lattice, a:

$$d_{hkl} = \frac{a}{\sqrt{h^2 + k^2 + l^2}} \tag{1}$$

$$2d \sin\theta = n\lambda \tag{2}$$

$$\tau = \frac{k\lambda}{\beta \cos\theta} \tag{3}$$

$$\sigma = \frac{\beta \cos\theta}{4} \tag{4}$$

where, d represent distance between parallel lattice planes with Miller Indices and h, k and l are the Miller indices of the respective Bragg refection and for the equation 3 and 4, τ denotes the crystallite size, k is shape factor with value of 0.9, λ represent wavelength of the radiation, β is the full width at hall maximum (FWHM) of the peak and θ is refraction angle (in radians).

TABLE 1. Crystallite Size, Lattice Parameter and Microstrain of YSZ thin film sintered at different temperature.

Sample Code	Sintering Temperature (°C)	τ (nm)	Reference τ (nm)	a (nm)	σ (nm)
S1	1100	2.1813	14.2, 19.2, 13.7, 17.3, 12, 6.6-17, 5 – 15	5.10398	0.1902
S2	1200	0.5875		5.139	0.04948
S3	1300	22.4725		5.10744	0.0069
S4	1400	14.0175		5.12042	0.0096
S5	1500	14.854		5.12462	0.0071

Surface Roughness and Grain Size

Figure 2 indicated the 3-dimensional AFM images of YSZ films sintered at different temperatures ranging from 1100 °C – 1500 °C. By looking at all the samples S1 to sample S5, the AFM images of S3 show a homogeneous surface without pores (Figure 2 (c)). While for the 3-dimensional AFM images of S4 and S5, the porosity surface and diminished island-look appear respectively.

Grain size can appear to affect the physical and chemical properties of a material. By analysing the grain size, the properties of a material can be understood much more in detail. The grain size of YSZ film sintered at different temperatures show nonuniform results from the grain size distribution which are 197.95 nm, 157.75 nm, 209.38 nm, 193.74 nm and 495.38 nm at 1100 °C, 1200 °C, 1300 °C, 1400 °C and 1500 °C respectively. The roughness of the sample is depended on the sintering temperature. The sintering temperature not only affects the surface but also affect the grain sizes of YSZ film. Table 2 tabulated the result of root mean square roughness (RMS) and average roughness (Ra) measured for the 5 samples. From the Table 2, it is shown that starting from 1100 °C, the RMS and Ra were increased from 12.44 nm and 5.812 nm to 36.25 nm and 25.67 nm respectively at first due to the fulfilment in sintering process and continue up to 1300 °C. After that, the RMS and Ra were decreased to 4.959 nm and 2.103 nm at 1400 °C which assuming from the melting distribution of the grain size. However, at 1500 °C, the RMS and Ra rose to 76.66 nm and 53.66 nm. Overall, it can be seen that the result of high sintering temperatures will shows some enlargement of grown size. However, there are also some mechanisms suggests

that large grains grown and small grain will shrink. Among all the 5 samples, the micrograph of AFM shows that S3 have the most uniform grain size with less porosity.

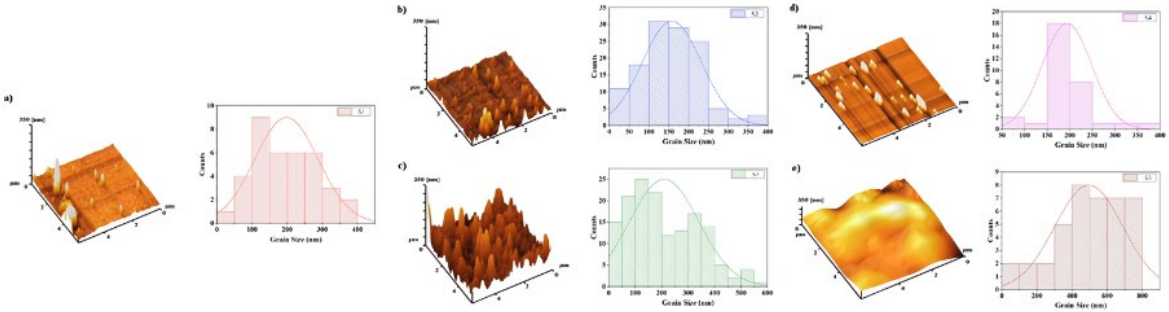

FIGURE 2. 3D AFM images (left) and corresponding grain size distribution (right) of YSZ film sintered at (a) 1100 °C, (b) 1200 °C, (c) 1300 °C, (d) 1400 °C, (e) 1500 °C.

TABLE 2. Root Mean Square Roughness (RMS), Average Roughness (Ra) and grain size of YSZ thin film sintered at different temperature.

Sample Code	Sintering Temperature (°C)	RMS (nm)	Ra (nm)	Grain Size (nm)	Reference Grain Size (nm)
S1	1100	12.44	5.812	197.95	-
S2	1200	25.05	12.6	157.75	50-70
S3	1300	36.25	25.67	209.38	1000
S4	1400	4.959	2.103	193.74	50 - 6000
S5	1500	76.66	53.66	495.38	-

Nucleation and Growth

The equation used to calculate the free energy are as shown below [8]:

$$r^*_{het} = -\frac{2T_m(a_1\gamma_{LN} + a_2\gamma_{NS} - a_2\gamma_{LS})}{3a_3\Delta H_f \Delta T} \tag{5}$$

$$\Delta G^*_{het} = \frac{4T_m^2(a_1\gamma_{LN} + a_2\gamma_{NS} - a_2\gamma_{LS})^3}{27a_3^2\Delta H_f^2 \Delta T^2} \tag{6}$$

$$\Delta G_{het} = a_3 \mathrm{r}^3 \frac{\Delta H_f \Delta T}{T_m} + a_1 \mathrm{r}^2 \gamma_{LS} + a_2(\mathrm{r}^2\gamma_{NS} - \mathrm{r}^2\gamma_{LN}) \tag{7}$$

Figure 3 (a) indicated the graph of free energy with varying in the radius of nucleus at 1500 °C which the value of ΔG_{het} is the total sum of both surface free energy, Δs and volume free energy, Δv. There are three principal modes of film growth are generally known as Frank-van der Merwe (FM) growth mode, Volmer-Weber (VW) growth mode and Stranski-Krastanov (SK) which named after their original investigators [9]. From the simulation result, the r^* will be 6.35nm at

1500 °C. By looking on the interfacial energy between YSZ nuclei and the substrate from the simulation result, the growth mode of the film growth can be identified. The surface energy per unit area of a nucleus, γ_{SL} = 0.73, γ_{SC} = 0.9, γ_{CL} = 0.13 and contact angle, θ = 70°. The simulation results favour the Volmer-Weber (VW) growth mode which the conditions 0°< θ< 90° and $\gamma_{SL} < \gamma_{SC} + \gamma_{CL}$ has fulfilled [9].

Figure 3 (b) shows the plot of $\Delta G^*$and r^*as a function of temperature at range of T = 0 − 2800K. From the graph itself tells that the $\Delta G^*$and r^*will increase with the increasing of temperature, the increase in the $\Delta G^*$and r^* become more obvious near the melting temperature as it rose significantly. This demonstrate that the temperature is an important factor that strongly influence the thin film growth. Temperature can influence the surface energy of the solid nucleus which eventually change the $\Delta G^*$and r^*. Figure 3 (c) indicated that the value of ΔG^*can be significantly smaller which up to range $10^{-15} - 10^{-18}$ for heterogeneous nucleation which change depending on the contact angle, θ. From the graph, it is observed that the ΔG^* is inversely proportional to the contact angle, θ which the ΔG^* will decrease with the increase of θ and the effect of θ on ΔG^* become less significant as the value of θ become higher. Consequently, the heterogeneous nucleation which having a much lower in value of ΔG^* than homogeneous nucleation would happen more often. The reason behind the lower value of ΔG^* can be explained from the contribution of interfacial energy between the substrate and nuclei that influence the free energy for the nuclei to form.

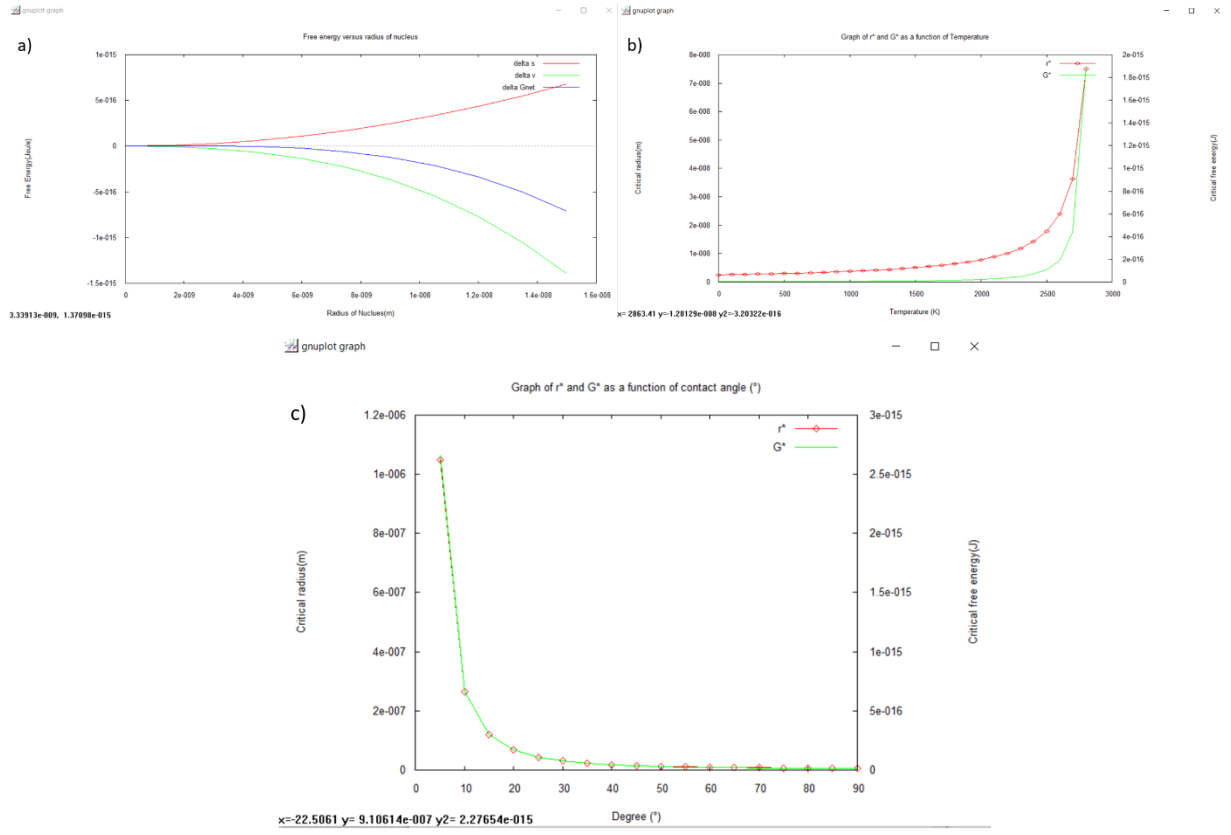

FIGURE 3. Graph of free energy ($\Delta s, \Delta v, \Delta G_{het}$) versus radius of nucleus at 1500 °C. (a)Graph of r^* and ΔG^* as a function of temperature. (b)Graph of $r^*$and ΔG^* as a function of contact angle.

IV. CONCLUSION

This work has initiated to focus on the initial stages of YSZ nucleation simulate using Microsoft Visual Basic. Meanwhile, the morphological and microstructure properties have been studied using AFM and XRD. From the simulation result, it is found that at 1500°C, the r^* will be 6.35nm and the simulation result favour the VW growth mode which the conditions $0° < \theta < 90°$ and $\gamma_{SL} < \gamma_{SC} + \gamma_{CL}$ has fulfilled. Meanwhile, the temperature and contact angle are also important factors that can strongly influence the thin film growth and affect r^* and ΔG^*. The increase in temperature gives a rise in r^* and ΔG^* while high contact angle will contribute to lower $r^*$and ΔG^*.

For the result from the AFM images, the morphological properties of samples at different sintering temperatures are studied. Some fluctuation results for the roughness parameter were observed but generally, the high sintering temperature will show some enlargement of grain size. Among all the 5 samples, S3 have the most uniform grain size with less porosity. In the meantime, the results of XRD indicated that the highest intensity peak appears with the hkl parameters of the different peak for all the samples were indexed to (111), (200), (220) and (311) indicating the YSZ thin films exhibit the cubic structure.

ACKNOWLEDGMENTS

This study has been supported by the UTM Encouragement Research (GUP IE : Q.J130000.3854.19J18).

REFERENCES

1. M.C. Roco (1999). Nanoparticles and Nanotechnology Research., 1(1), 1–6. doi:10.1023/a:1010093308079
2. Kumar, A., Yadav, N., Bhatt, M., Mishra, N., Chaudhary, P., and Singh, R., (2015). Sol-Gel Derived Nanomaterials and It's Applications: A Review. Research Journal of Chemical Sciences, 5, 1-6.
3. Maridurai, T, Balaji, D and Sagadevan, S., (2016). Synthesis and Characterization of Yttrium Stabilized Zirconia Nanoparticles. Materials Research, 19(4), 812–816. doi:10.1590/1980-5373-MR-2016-0196
4. Vonk, V., Khorshidi, N., Stierle, A., and Dosch, H., (2013). Atomic structure and composition of the yttria-stabilized zirconia (111) surface. Surface Science, Vol 612, 69–76. doi:10.1016/j.susc.2013.02.014
5. Joo, J., Yu, T., Kim, Y., Park, H., Wu, F., Zhang, J., and Hyeon, T., (2003). Multigram Scale Synthesis and Characterization of Monodisperse Tetragonal Zirconia Nanocrystals. Journal of the American Chemical Society, Vol 125(21), 6553–6557.
6. Holzwarth, U., and Gibson, N., (2011). The Scherrer equation versus the 'Debye–Scherrer equation'. Natural Nanotechnology, Vol 6, 534.
7. Mote, V., Purushotham, Y., and Dole, B., (2012). Williamson-Hall analysis in estimation of lattice strain in nanometer-sized ZnO particles. Journal of Theoretical and Applied Physics, 6(1), 6. doi:10.1186/2251-7235-6-6

8. Thanh, N., Maclean, N., and Mahiddine, S., (2014). Mechanisms of Nucleation and Growth of Nanoparticles in Solution. Chemical Reviews, Vol 114(15), 7610–7630. doi:10.1021/cr400544s
9. Oura, K., Katayama, M., Zotov, A., Lifshits, V., and Saranin, A., (2003). Growth of Thin Films. In: Surface Science. Advanced Texts in Physics. Springer, Berlin, Heidelberg. https://doi.org/10.1007/978-3-662-05179-5_14